The absence of a discommensuration lattice in the incommensurate phase of Rb_2ZnCl_4

1999 J. Phys.: Condens. Matter 11 1639

(http://iopscience.iop.org/0953-8984/11/7/001)

J. Phys.: Condens. Matter **11** (1999) 1639–1655. Printed in the UK PII: S0953-8984(99)96577-3

The absence of a discommensuration lattice in the incommensurate phase of Rb_2ZnCl_4

A Yu Babkevich and R A Cowley

Department of Physics, Clarendon Laboratory, Parks Road, Oxford OX1 3PU, UK

Received 3 August 1998

Abstract. X-ray scattering close to the lock-in temperature T_L has been measured as a function of temperature to investigate whether the discommensuration lattice is a useful description of the structure of Rb_2ZnCl_4. We review different models for the incommensurate structure and discuss how they might be distinguished by a scattering experiment. Our results are compared with earlier published x-ray measurements and with those obtained from nuclear spin-resonance techniques. All of the x-ray results suggest that higher harmonics of the scattering measured in the a^*/c^* and b^*/c^* planes are much weaker than predicted by the abrupt-discommensuration model. We conclude from the measurements that this theory does not provide an adequate description of the experimental results close to the lock-in transition.

1. Introduction

Rubidium tetrachlorozincate, Rb_2ZnCl_4, on cooling to a temperature $T_I \approx 303$ K undergoes a structural phase transition from a paraelectric normal (regular) phase to a phase which is incommensurably modulated. On further cooling, the wave vector of the incommensurate modulation changes until it locks in to a commensurate wave vector at $T_L \approx 192$ K, and the structure becomes a commensurate ferroelectric phase [1, 2]. There is now a generally good understanding of the structure and properties of Rb_2ZnCl_4 at temperatures close to T_I [3]. The critical phenomena have been measured [4, 5], and the results for the temperature dependence of primary and secondary order parameters are in accord with theoretical expectations.

The situation is much less satisfactory close to the lock-in transition temperature, T_L. There is an appealingly simple picture of the transition in Rb_2ZnCl_4 and in other materials with similar phase transitions as arising from an instability of the low-temperature phase against the spontaneous creation of discommensurations (also termed solitons, domain walls, phase distortions or phase dislocations) [6]. The structure of the incommensurate phase is predicted to consist of regions of constant phase φ (the commensurate regions) separated by equally spaced regions of rapidly changing phase (the discommensurations) in which φ changes by $2\pi/p$ (p is an integer, such that $p\boldsymbol{q}_c = \boldsymbol{G}$ where $\boldsymbol{G}$ is a reciprocal-lattice vector and $\boldsymbol{q}_c$ is the commensurate wave vector to which the lock-in transition actually takes place); the spacing between the discommensurations steadily increases and consequently their concentration decreases as T_L is approached from above [6–8]. The basic assumption of the discommensuration description is that the displacements of the atoms can be represented in terms of an amplitude $A(\boldsymbol{r})$ and phase $\varphi(\boldsymbol{r})$ as

$$U(\boldsymbol{r}) = A(\boldsymbol{r})\cos(\boldsymbol{q}_c \cdot \boldsymbol{r} + \varphi(\boldsymbol{r}))$$

0953-8984/99/071639+17$19.50

where the lattice vector $\boldsymbol{r}$ has x-, y-, z-components. This type of theory has been very successful in describing the properties of lattice strained epilayers and of two-dimensional films [9], but its usefulness in describing incommensurably modulated phases in three-dimensional crystals is not yet established. The reason for the uncertainty is that a regular discommensuration lattice gives rise to a characteristic diffraction pattern [10] which has not yet been observed [11] although electron microscopy [12, 13] and nuclear magnetic resonance results [14–16] have been interpreted as providing evidence for the existence of the discommensurations in Rb_2ZnCl_4.

The detailed structure of the modulated phase in Rb_2ZnCl_4 has been determined from neutron [17, 18] and x-ray scattering [11, 19–26] measurements of the intensities of the first-order incommensurate peaks. In this paper our intention is to re-examine the x-ray scattering close to T_L to investigate whether the discommensuration lattice is a useful description of the structure of materials close to the lock-in type of phase transition. In the next section we review different models for the incommensurate structure and how they might be distinguished by a scattering experiment. Predictions of the theory will be compared in section 3 with our x-ray scattering experiments performed on Rb_2ZnCl_4. We shall show that a discommensuration lattice is not an appropriate description of the experimental results. In section 4 these results are compared with the x-ray measurements of others and with those obtained from nuclear spin-resonance techniques, and finally the results are summarized in section 5.

2. Scattering from incommensurably modulated phases

At high temperatures, above T_I, the atoms are situated at the positions $\boldsymbol{R}(\nu\mu)$, where the label ν describes the unit cell, μ labels the μth type of atom within the unit cell and

$$\boldsymbol{R}(\nu\mu) = \boldsymbol{R}(\nu) + \boldsymbol{R}(\mu). \tag{1}$$

The atoms are displaced from these positions in the incommensurably modulated phase by displacements which can be written in the form

$$\boldsymbol{U}(\nu\mu) = \sum_{n=0}^{\infty} \boldsymbol{u}(n\mu)\sin(n\boldsymbol{q}\cdot\boldsymbol{R}(\nu) + \Phi(n\mu)) \tag{2}$$

where we have assumed a one-dimensional modulation described by a wave vector $\boldsymbol{q}$, and the $\boldsymbol{u}(n\mu)$ are the real amplitudes of the Fourier coefficients of the displacements and the $\Phi(n\mu)$ are the phases of the displacements. In principle the phases of the displacements depend on the component of the displacement, and differ for U_x, U_y and U_z. In the interests of simplicity we have not included these suffices but they are readily included in the theory. The unusual features of an incommensurate crystal are that all of the displacements, $\boldsymbol{U}(\nu\mu)$, are different and that in principle there are an infinite number of amplitudes $\boldsymbol{u}(n\mu)$ and phases $\Phi(n\mu)$ needed to describe the displacements. Nevertheless the sum in equation (2) is usually dominated by a few low-order terms in n.

We follow first the interpretation by Perez-Mato *et al* [27] to develop the theory in the three-dimensional space. We introduce a new variable $v = \boldsymbol{q}\cdot\boldsymbol{R}(\nu)$ which is similar to the continuous 'internal' variable used by Perez-Mato *et al*. $\boldsymbol{U}(v\mu)$ is periodic in v with a period of 2π and so we only need to consider the values of v between 0 and 2π. If the wave vector $\boldsymbol{q}$ is incommensurate, the values of v form a discrete set between 0 and 2π.

The structure factor amplitude for the scattering for a wave-vector transfer $\boldsymbol{Q}$ is given by

$$F(\boldsymbol{Q}) = \frac{1}{N}\sum_{\nu\mu} f^{\mu}(\boldsymbol{Q})\exp[\mathrm{i}\boldsymbol{Q}\cdot(\boldsymbol{R}(\nu\mu) + \boldsymbol{U}(\nu\mu))] \tag{3}$$

where $f^{\mu}(\boldsymbol{Q})$ is the x-ray form factor or coherent neutron scattering length of an atom of type μ, and N is the number of unit cells in the high-temperature structure. The structure factor for a wave-vector transfer, $\boldsymbol{Q} = \boldsymbol{G} + m\boldsymbol{q}$, with $\boldsymbol{G}$ a reciprocal-lattice vector of the high-temperature structure is then [27]

$$F(\boldsymbol{Q}) = \sum_{\mu} f^{\mu}(\boldsymbol{Q}) g^{\mu}(\boldsymbol{Q}) \exp(\mathrm{i}\boldsymbol{Q} \cdot \boldsymbol{R}(\mu)) \tag{4}$$

where the 'atomic modulation factor' is

$$g^{\mu}(\boldsymbol{Q}) = \frac{1}{2\pi} \int_0^{2\pi} \exp[\mathrm{i}(\boldsymbol{Q} \cdot \boldsymbol{U}(v\mu) + mv)] \, \mathrm{d}v \tag{5}$$

where m is an integer and denotes an index of an incommensurate Bragg reflection. To simplify the analysis we have neglected thermal motions, but the effect of the Debye–Waller factor will be discussed briefly in section 4. We rewrite equation (5) as

$$g^{\mu}(\boldsymbol{Q}) = \frac{1}{2\pi} \int_0^{2\pi} \left(1 + \mathrm{i}\boldsymbol{Q} \cdot \boldsymbol{U}(v\mu) - \frac{(\boldsymbol{Q} \cdot \boldsymbol{U}(v\mu))^2}{2} + \cdots \right) \exp(\mathrm{i}mv) \, \mathrm{d}v. \tag{6}$$

When equation (2) is then substituted into equation (6), the term of first order in the displacement becomes

$$g_1^{\mu}(\boldsymbol{Q}) = -\frac{1}{2} \sum_{n=0}^{\infty} \boldsymbol{Q} \cdot \boldsymbol{u}(n\mu) \left[\delta(n+m) \exp(\mathrm{i}\Phi(n\mu)) - \delta(n-m) \exp(-\mathrm{i}\Phi(n\mu)) \right]. \tag{7}$$

The result suggests that the intensity of the mth-order satellite with $\boldsymbol{Q} = G + m\boldsymbol{q}$ is given by the square of mth-order displacements $|\boldsymbol{u}(m\mu)|^2$. Unfortunately the situation is more complex as can be seen by considering the quadratic term in the expansion, equation (6). When equation (2) is substituted into this term and the integration over v performed, the results are the delta functions $\delta(n_1 + n_2 \pm m)$, where n_1 and n_2 are the indices resulting from the expansion of the two $\boldsymbol{U}(v\mu)$ in terms of n Fourier components. As a result there is a contribution to, say, $m = 1$ when $n_1 = -2$ and $n_2 = 1$. Extension of this analysis then leads to the conclusion that, in principle, all Fourier coefficients contribute to the intensity of every incommensurate reflection and that consequently the analysis becomes extremely complex.

Progress can be made only if approximations are made. One approximation is to assume that the amplitude of the Fourier components decreases rapidly with n so that only the leading terms need to be considered for any incommensurate peak. For $m = 1$ the leading term has $n = \pm 1$, while for $m = 2$ there are two types of term: one from the first-order term in equation (6) which has $n = \pm 2$, and other from the second term which has $n_1 = n_2 = \pm 1$. The former is the scattering from the second-order distortion and the latter is that from the second diffraction harmonic of the first-order distortion. These different contributions make the analysis of the diffraction pattern from incommensurate phases very difficult to interpret for the peaks with $|m| > 1$. Indeed, there have been only a few attempts to extract the second- and higher-order displacements $\boldsymbol{u}(n\mu)$ for $n > 1$ [28]. The situation is simpler for magnetic systems [29], because in this case the magnetic scattering of neutrons does not produce the diffraction harmonics and the cross section is similar to that given by the small-$\boldsymbol{U}$ approximation of equation (7). Equation (6) shows that the relative contributions of the diffraction harmonics and higher-order displacements depend differently on the wave-vector transfer $\boldsymbol{Q}$. The contributions to the structure factor for $m = 2$ vary as $|\boldsymbol{Q}|^2$ for the primary order parameter $n_1 = n_2 = \pm 1$ and as $|\boldsymbol{Q}|$ for the secondary order parameter $n = \pm 2$. The diffraction harmonics will then tend to be the largest contribution to the scattering for large $|\boldsymbol{Q}|$ while the secondary order parameters dominate for small $|\boldsymbol{Q}|$.

Another approximation is based on using the Jacobi–Anger generating function for the Bessel function:

$$\exp(\mathrm{i}x\sin p) = \sum_{M=-\infty}^{\infty} \exp(\mathrm{i}Mp) J_M(x) \tag{8}$$

where $J_M(x)$ is the Mth-order Bessel function. This expansion is an alternative to the direct expansion of the exponential for small x used to obtain equation (6). When equation (2) is substituted into equation (5) and the identity (8) is used, then

$$g_\mu(\boldsymbol{Q}) = \int_0^{2\pi} \prod_{n=0}^{\infty} \left[\sum_{M=-\infty}^{+\infty} J_M(\boldsymbol{Q}\cdot\boldsymbol{u}(n\mu)) \exp[\mathrm{i}M(n\nu + \Phi(n\mu))] \right] \exp(\mathrm{i}m\nu)\, \mathrm{d}\nu. \tag{9}$$

The two approaches both lead to an infinite series of terms but differ in the way in which higher-order terms are incorporated. It is *a priori* unclear for which expansion the lowest-order terms give the best approximation to the scattering.

Another approach which has been developed for use close to the lock-in transition [6, 7] is that of describing the displacements in the incommensurate phase in terms of those of the *commensurate* lock-in phase. The displacements are then a homogeneous modification of the displacements of the lock-in phase. We shall assume for simplicity that the displacements of the commensurate phase are described in terms of a single wave vector, $\boldsymbol{q}_c$, and are given by

$$\boldsymbol{U}_c(\nu\mu) = \boldsymbol{u}_c(\mu)\sin(\boldsymbol{q}_c\cdot\boldsymbol{R}(\nu) + \Phi_c(\mu)) \tag{10}$$

where $\boldsymbol{u}_c(\mu)$ and $\Phi_c(\mu)$ are the amplitudes and phases, similar to those introduced in equation (2). The commensurate phase has p different domains whose structures differ only in that the phases of the displacements are all increased by multiples of $2\pi/p$.

The structure of the *incommensurate* phase consists of a regular sequence of these domains separated from one another by phase discommensurations. Each discommensuration has a width λ and a phase change by $2\pi/p$ across the discommensuration, and is separated from the next discommensurations by on average the distance b. A displacement pattern of this form can be written as

$$\boldsymbol{U}_c(\nu\mu) = A(\nu)\boldsymbol{u}_c(\mu)\sin(\boldsymbol{q}_c\cdot\boldsymbol{R}(\nu) + \varphi(\nu) + \Phi_c(\mu)) \tag{11}$$

where $\varphi(\nu)$ is the variation of the phase of the commensurate distortion across each unit cell and $A(\nu)$ is the variation of the amplitude. The basic assumption of the method is that $A(\nu)$ and $\varphi(\nu)$ do not depend on the atom type μ, and hence the system can be treated as a continuum. There have been many calculations of the variation of $A(\nu)$ and $\varphi(\nu)$ beginning with the work of McMillan [6] and of Bak and Emery [7] and continuing later [8, 30]. We shall review only the relevant results. Firstly the amplitude variations are small and relatively unimportant so we may neglect them [31]. Secondly if the phase increases by $2\pi/p$ across discommensurations separated by a distance b in the direction of $\boldsymbol{q}_c$, which we shall take as the z-axis, then [10]

$$\varphi(z) = \varphi_0 + \frac{2\pi}{p}J + \Psi(z - Jb) \tag{12}$$

where J is the integer closest to z/b, φ_0 is a constant and $\Psi(z)$ is the solution for the shape of a single discommensuration which can be obtained from the sine–Gordon equation [32] as

$$\Psi(z) = \frac{4}{p}\tan^{-1}(\exp(z/\lambda)). \tag{13}$$

As $T \to T_L$ the number of the discommensurations decreases, so b increases while the width of the discommensurations, λ, varies only slightly.

Table 1. The positions and indexing of the incommensurate reflections of Rb_2ZnCl_4. h, k, l are the Miller indices; ξ is the position of the satellites in a $\boldsymbol{c}^*$-direction.

Position ($\delta = 0.0169$)			$\boldsymbol{G} \pm m(\frac{1}{3} - \delta)\boldsymbol{c}^*$			$\boldsymbol{G} \pm m(\frac{2}{3} + \delta)\boldsymbol{c}^*$		
h	k	ξ	$\pm$	l	m	$\pm$	l	m
6	0	0	+	0	0	+	0	0
6	0	0.5315	+	−2	8	+	6	−8
6	0	0.5822	+	−1	5	+	4	−5
6	0	0.6329	+	0	2	+	2	−2
6	0	0.6836	+	1	−1	+	0	1
6	0	0.7343	+	2	−4	+	−2	4
6	0	0.7850	+	3	−7	+	−4	7
6	0	1	+	1	0			
6	0	1.2150	+	−1	7	−	6	−7
6	0	1.2657	+	0	4	−	4	−4
6	0	1.3164	+	1	1	−	2	−1
6	0	1.3671	+	2	−2	−	0	2
6	0	1.4178	+	3	−5	−	−2	5
6	0	1.4685	+	4	−8	−	−4	8
6	0	2	+	1	0	+	2	0
Position ($\delta = 0.0169$)			$\boldsymbol{G} \pm (\frac{1}{3} - \delta(1 + 3I))\boldsymbol{c}^*$			$\boldsymbol{G} \pm (\frac{2}{3} + \delta(1 + 3I))\boldsymbol{c}^*$		
h	k	ξ	$\pm$	l	I	$\pm$	l	I
6	0	0	+	0	0	+	0	0
6	0	0.5315	−	1	−3	+	0	−3
6	0	0.5822	−	1	−2	+	0	−2
6	0	0.6329	−	1	−1	+	0	−1
6	0	0.6836	−	1	0	+	0	0
6	0	0.7343	−	1	1	+	0	1
6	0	0.7850	−	1	2	+	0	2
6	0	1						
6	0	1.2150	+	1	2	−	2	2
6	0	1.2657	+	1	1	−	2	1
6	0	1.3164	+	1	0	−	2	0
6	0	1.3671	+	1	−1	−	2	−1
6	0	1.4178	+	1	−2	−	2	−2
6	0	1.4685	+	1	−3	−	2	−3
6	0	2						

The structure factor for the scattering can be calculated by substituting equations (12) and (13) into equation (11) and hence into equation (5). The results are necessarily complex and can only be evaluated numerically.

Alternatively, the expansion of equation (5) for small displacements can be used when the summations can be performed analytically. Firstly scattering occurs when [10]

$$\boldsymbol{Q} = \boldsymbol{G} \pm q_c(1 - \delta p(1 + Ip)) \tag{14}$$

where I is any positive or negative integer, $\delta = \pm c/b$ is the small 'mismatch parameter' and the positive sign is taken if the discommensurations advance the phase at each discommensuration along the crystal. If this theory is valid, b is large, and the intensity is largest for $I = 0$ and the scattering occurs at wave vectors around each particular lock-in wave vector. They are the same wave vectors as occurred in the previous description of the scattering. In the former description the wave-vector transfer of the mth-order satellite has $\boldsymbol{Q} = \boldsymbol{G} \pm m\boldsymbol{q}_m$, where for

Rb_2ZnCl_4 [11, 23] the modulation wave vector is $\boldsymbol{q}_m = (\frac{1}{3} - \delta)\boldsymbol{c}^*$. The discommensuration analysis gives the wave-vector transfers as $\boldsymbol{Q} = \boldsymbol{G} \pm (\frac{1}{3} - \delta(1 + 3I))\boldsymbol{c}^*$ because $p = 3$ and $\boldsymbol{q}_c = \frac{1}{3}\boldsymbol{c}^*$ for Rb_2ZnCl_4; both m and I are integers. In table 1 we list the correspondence between the two labellings for some of the scattering wave vectors observed for Rb_2ZnCl_4.

An expression for the atomic modulation factor can be obtained from the first term in equation (6) as

$$g_\mu(\boldsymbol{Q}) = -\frac{1}{2}(\boldsymbol{Q} \cdot \boldsymbol{u}_c(\mu)) \exp(\pm \mathrm{i}\Phi_c(\mu)) F(\boldsymbol{Q} - \boldsymbol{G} \pm \boldsymbol{q}_c) \tag{15}$$

where $F(\boldsymbol{Q})$ is the form factor of the discommensuration [10]:

$$F(Q) = \frac{1}{b}\int_{-b/2}^{b/2} \exp(\mathrm{i}Qz - \Psi(z))\, \mathrm{d}z \tag{16}$$

which depends on the structure of the discommensuration, but close to T_L the theory gives $b \gg \lambda$, the abrupt-discommensuration limit, when $F(Q)$ can be approximated as [10]

$$F(Q) = \left[\pi\left(\frac{1}{p} + I\right)\right]^{-1} \sin\left(\frac{\pi}{p}\right) \exp\left(-\frac{\mathrm{i}\pi}{p}\right). \tag{17}$$

Since this theory is appropriate only if b is large and the wave vectors $\boldsymbol{Q} - \boldsymbol{G}$ are close to $\boldsymbol{q}_c$, the relative intensity of the scattering for different integers, I, is determined by the form factors of the discommensurations given by equation (17). Since this factor is the same for all reciprocal-lattice vectors, $\boldsymbol{G}$, this model predicts that the relative intensities of the different scattering peaks are the same around each reciprocal-lattice vector. Furthermore, since the model is valid only if b is much larger than λ, equations (16) and (17) predict for $p = 3$ that the relative intensities for $I = -2, -1, 0, 1, 2$ are $\frac{1}{25}{:}\frac{1}{4}{:}1{:}\frac{1}{16}{:}\frac{1}{49}$.

This approach has assumed that the distortions are small so that the exponential can be expanded only to first-order terms, and has used an approximate way of calculating all of the higher-order distortions $\boldsymbol{U}(n\mu)$ in equation (2).

2.1. Superspace formalism and intensity calculation

The theory and calculations for incommensurably modulated crystals are conveniently performed using superspace groups as developed by de Wolff, Janner and Janssen [33–35], and by Yamamoto and Nakazawa [36, 37]. The development is equivalent to that of Perez-Mato *et al* [27] but for completeness we give the more general expressions needed for our numerical calculations for Rb_2ZnCl_4 . If there is a single incommensurate wave vector $\boldsymbol{q}_m$ and the occupation probability of each site is one, the intensity expression given by Yamamoto can be written as

$$F(hklm) = \sum_{\mu,(R|\tau)} \int_0^1 \mathrm{d}\bar{x}_4^\mu \; f^\mu(\boldsymbol{H}) \exp\{-6\pi^2 U_{eq}^\mu + 2\pi\mathrm{i}\boldsymbol{H}([R]\boldsymbol{x}^\mu(\bar{x}_4^\mu) + \tau^\mu)\} \tag{18}$$

where μ runs over all non-equivalent atoms. In this expression the wave-vector transfer $\boldsymbol{H} \equiv \boldsymbol{Q}/2\pi$ is specified by the four-dimensional vector of integers $\boldsymbol{H} = (hklh_4) = (h_1h_2h_3h_4)$ and $f^\mu(\boldsymbol{H})$ is the atomic form factor written earlier as $f^\mu(\boldsymbol{Q})$. B_{eq}^μ is the isotropic thermal parameter.

The positions of the atoms are written in terms of the coordinates along the basis vectors, $\boldsymbol{a}_i$, of the four-dimensional space and so for $i = 1, 2, 3$

$$x_i^\mu \boldsymbol{a}_i = R_i(\mu) + u_i(v\mu) \tag{19}$$

while for $i = 4$

$$\bar{x}_4^\mu = \frac{v}{2\pi} + \frac{1}{2\pi}\boldsymbol{q}\cdot\boldsymbol{u}(v\mu). \tag{20}$$

Substitution of these results into equation (18) and neglect of the Debye–Waller factor gives an expression which is identical to that given in equation (4).

The high-temperature space group of Rb_2ZnCl_4 is P_{mcn} and the modulation wave vector $\boldsymbol{q}$ is along the c-direction $\boldsymbol{q} = (0, 0, \xi)$. The superspace group of the modulated phase is $P_{ss\bar{1}}^{P_{mcn}}$ [23], and there are six non-equivalent atoms in the unit cell. The coordinates of the equivalent atoms are given by [38]:

$$\begin{array}{ll} x, y, z, w & -x+\frac{1}{2}, -y+\frac{1}{2}, z+\frac{1}{2}, w \\ x+\frac{1}{2}, -y, -z, -w+\frac{1}{2} & -x, y+\frac{1}{2}, -z+\frac{1}{2}, -w+\frac{1}{2} \\ -x, -y, -z, -w & x+\frac{1}{2}, y+\frac{1}{2}, -z+\frac{1}{2}, -w \\ -x+\frac{1}{2}, y, z, w+\frac{1}{2} & x, -y+\frac{1}{2}, z+\frac{1}{2}, w+\frac{1}{2}. \end{array}$$

The symmetry of the modulated structure imposes conditions on the Bragg reflections, as given by Yamamoto [38]:

$h = 2n$	for $h000$
$k = 2n$	for $0k00$
$h + k = 2n$	for $hk00$
$l = 2n$	for $00lm$
$m = 2n$	for $0klm$
$l + m = 2n$	for $h0lm$

where $m \equiv h_4$ is the index m of the Bragg reflection $\boldsymbol{Q} = G + m\boldsymbol{q}$ as given in the first column of table 1. The experimental measurements were mostly performed with the scattering vector in the $(h0l)$ plane, for which case the conditions on the reflections show that for reflections in that plane the unit cell in the high-temperature phase can be treated as being of length $c/2$, and the modulation wave vector as $\boldsymbol{q} = (0, 0, 1 - \xi)$. The indices for the reflections labelled in this way are listed in columns 2 and 4 of table 1.

The lowest-order ($n = 1$) displacements of the atoms in the modulated phase were determined [23] in the form

$$u(\mu v) = a_0^\mu/2 + a_1^\mu \cos(v) + b_1^\mu \sin(v) \tag{21}$$

which is an alternative form of equation (2) but with the amplitude and phase written in terms of cosines and sines. The intensities of the Bragg reflections for $m = 0$ and 1 and of the corresponding diffraction harmonics for larger m were calculated by substituting equation (21) into equation (18) and using the symmetry to sum over all of the atoms in the unit cell.

3. Experimental measurements

3.1. The sample

The sample chosen for a study of the structure of the incommensurate phases was Rb_2ZnCl_4. Large single crystals are available, the incommensurate phase occurs over a wide and convenient temperature range and there have been many other studies of this material. The crystals

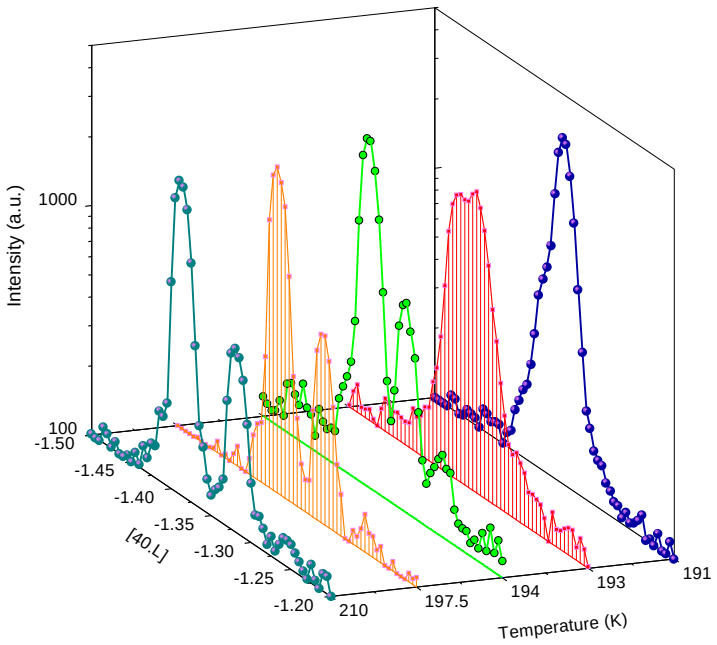

Figure 1. The temperature variation of the intensities observed for wave vectors $40L$ on cooling towards T_L.

used were grown by Dr J Y Gesland at the Université du Maine and by Dr K Hamano at the Tokyo Institute of Technology and were previously studied at temperatures close to T_I [5]. The crystals had a mosaic spread of about 0.01°. The crystal structure in the high-temperature phase has lattice constants measured at 200 K as $a = 0.7253$ nm, $b = 1.2670$ nm and $c = 0.9221$ nm. The incommensurate wave vector is along $\boldsymbol{c}^*$ and in the locked-in commensurate phase below 192 K, $\boldsymbol{q}_c$ is $\frac{1}{3}\boldsymbol{c}^*$.

Experimental measurements were made in the extended-face geometry with faces perpendicular to either the $\boldsymbol{b}^*$- or $\boldsymbol{a}^*$-directions. In the former case the scattered intensities were measured in the $\boldsymbol{a}^*/\boldsymbol{c}^*$ plane and in the latter case in the $\boldsymbol{b}^*/\boldsymbol{c}^*$ plane.

3.2. The x-ray measurements

The x-ray source was a Stoe rotating anode with a Cu target operating at 6 kW. The collimations of the incident and scattered beams were both controlled by pyrolytic graphite crystals reflecting from the $(0002)_h$ plane. This arrangement gave a high flux which enabled weak reflections to be measured but sufficient resolution to separate the different satellite reflections.

The samples were mounted in a closed-cycle cryostat and aligned with either the $h0l$ or $0kl$ reflections in the scattering plane of a two-axis diffractometer. Silicon diode temperature sensors were used to control the temperature with an absolute accuracy of ± 0.5 K. A temperature controller gave the stability of the temperature control to ± 2.5 mK. The software was designed so as to give a smooth temperature change and such that the temperature has an overshoot of less than 0.1 K.

The diffractometer was controlled by SPEC software and the wave-vector transfer $\boldsymbol{Q}$ was scanned for ξ along the lines $(h0\xi)$ or $(0k\xi)$ for the accessible regions of reciprocal space.

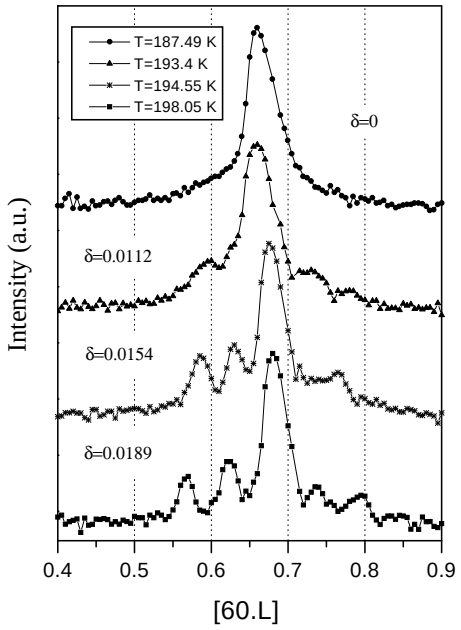

Figure 2. The temperature variation of the intensity of the 60L satellite reflections (sample 1).

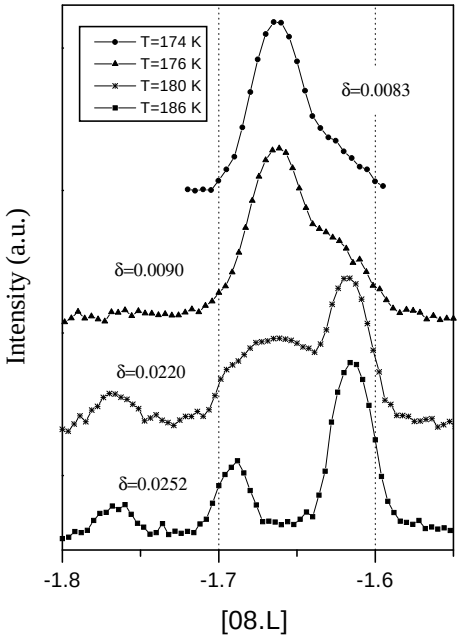

Figure 3. The temperature variation of the intensity of the 08L satellite reflections (sample 2).

Table 2. The ratio of the satellite intensities at $T = 195.54$ K. h, k, l are the Miller indices; I has the same meaning as in table 1.

Indices	Observed/ calculated	+/−	$I(-2)/I(0)$	$I(-1)/I(0)$	$I(0)$	$I(1)/I(0)$	$I(2)/I(0)$
400	Observed	−	0.0151	0.0134	577	0.0023	0.0014
	Calculated		10^{-6}	0.0043		10^{-5}	10^{-10}
$40\bar{2}$	Observed	+	—	4.72	18	0.0011	—
	Calculated		10^{-5}	2.2899		0.0017	10^{-9}
$50\bar{2}$	Observed	−	0.011	0.0865	173	0.0092	—
	Calculated		10^{-4}	0.5		0.0041	10^{-7}
600	Observed	+	0.0085	0.012	1106	0.0048	0.0039
	Calculated		10^{-5}	0.0028		10^{-4}	10^{-8}
600	Observed	−	0.0093	0.014	1638	0.0027	0.0038
	Calculated		10^{-5}	0.0028		10^{-4}	10^{-8}
$60\bar{2}$	Observed	+	0.009	0.11	387	0.0089	0.0048
	Calculated		10^{-4}	0.51		0.0022	10^{-7}
Discommensuration model	Calculated		0.04	0.25	1	0.0625	0.0204

Typical results at several different temperatures are shown in figure 1, and it is clear that the relative intensities of the satellites are not changing rapidly with temperature as the sample is cooled towards T_L. The diffracted intensities were measured at 16 different temperatures in the range 210–172 K on cooling. Because there was evidence for the commensurate phase and

incommensurate phase coexisting close to T_L, most of the measurements were made between 193 and 200 K and some distributions of the intensity for the $(h0l)$ plane are shown in figure 2 and for the $(0kl)$ plane in figure 3.

The results in figure 2 show a sequence of satellite peaks around each of the lock-in wave vectors. These peaks were fitted to pseudo-Voigt function (which is linear convolution of a Gaussian and a Lorentzian) to obtain the integrated intensities and the results are listed in table 2 giving the intensity for the most intense peak, $I = 0$, and the ratios of the intensities of the satellite peaks with $I = \pm 1$ and ± 2 to the intensity of the $I = 0$ peak. Since all of the peaks in each group have similar wave-vector transfers, the Lorentz, polarization, absorption, form factors and geometrical corrections are similar within each group of peaks.

Table 3. The ratio of satellite intensities at $T = 186$ K. h, k, l are the Miller indices; ξ is the position of the satellites in the c^*-direction; m has the same meaning as in table 1.

Position ($\delta = 0.0252$)				Intensity	
h	k	ξ	$hklm$	Measured	Calculated
0	8	−1	$08\bar{1}0$	12743	8250
0	8	−1.2325	$080\bar{4}$	14	0.05
0	8	−1.3837	$08\bar{2}2$	38	0.25
0	8	−1.6163	$08\bar{1}\bar{2}$	138	126
0	8	−1.7675	$08\bar{3}4$	10	0.04
0	8	−2	$08\bar{2}0$	6089	8389
0	8	−2.3837	$08\bar{3}2$	40	23
0	9	−0.6163	$090\bar{2}$	15	0.09
0	9	−0.7675	$09\bar{2}4$	5	0.03
0	9	−1	$09\bar{1}0$	21375	20424
0	9	−1.2325	$09\bar{4}0$	9	0.02
0	9	−1.3837	$09\bar{2}2$	84	11
0	9	−1.6163	$09\bar{1}\bar{2}$	59	18
0	9	−2	$09\bar{2}0$	30352	32384
0	10	0	0 10 00	23551	28228
0	10	−0.3837	0 10 $\bar{1}2$	7	27
0	10	−0.6163	0 10 $0\bar{2}$	126	73
0	10	−1	0 10 $\bar{1}0$	3524	3689
0	10	−1.3837	0 10 $\bar{2}2$	51	48
0	10	−1.6163	0 10 $\bar{1}\bar{2}$	7	43
0	10	−2	0 10 $\bar{2}0$	697	471
0	12	−2	0 12 $\bar{2}0$	356	358
0	12	−2.3837	0 12 $\bar{3}2$	53	3
0	12	−2.6163	0 12 $\bar{2}\bar{2}$	118	23
0	12	−2.7675	0 12 $\bar{4}4$	24	0.03
0	12	−3	0 12 $\bar{3}0$	1136	1125

Figure 3 and table 3 show the results for the $(0kl)$ plane. In this plane the symmetry of the primary distortions is such that the structure factor for the satellite reflections is zero for $\boldsymbol{Q} = \boldsymbol{G} \pm m\boldsymbol{q}$, when m is odd. Consequently the only satellite reflections expected are those with m even and in the other notation with I odd. The results in figure 3 show that there is a peak with $\xi \approx -1.69$ corresponding to $m = 1$ or $I = 0$ but that it is weaker than the $I = -1$ peak with $\xi \approx -1.62$. We consider that the former peak may arise from multiple scattering and illustrates the difficulty of reliably measuring weak satellite intensities. The intensities of the reflections observed along the lines $(0k\xi)$ with $k = 12, 10, 9$ and 8 are listed in table 3.

The samples used for the measurements in the a^*/c^* and the a^*/b^* planes are of different origin. In the first case, the temperature of the lock-in transition was about 192 K while in the second one it was about 178 K. This discrepancy could be due to different concentrations of impurities or defects in the samples. A lower transition temperature has been ascribed to the presence of defects [25, 39, 40].

It is difficult to estimate the errors of the experimental results in tables 2 and 3. Accurately measuring intensities which differ by orders of magnitude is extremely difficult because the most intense peaks may be reduced by extinction while multiple scattering may contribute to the intensities of the weak peaks. Both of these effects tend to reduce the differences between the measured intensities of the strong and weak reflections.

3.3. The results

The most important aspect of our results is summarized in table 2. The model of the scattering provided by the discommensuration theory combined with the expansion of the exponential in equation (5) for small $\boldsymbol{U}(v\mu)$ gives the result that the ratios $I(-2)/I(0), \ldots, I(2)/I(0)$ are the same for all of the groups of satellite reflections. The results, table 2, show that this is not the case, because $I(-1)/I(0)$ varies between 4.7 and 0.013 while $I(1)/I(0)$ varies between 0.009 and 0.0011.

One reason for this discrepancy is the presence of the diffraction harmonics of the primary distortion. For example, the scattering from the $I = -1, m = 2$ satellite has a contribution from the second diffraction harmonic as well as from the second-order distortions. The intensities of the diffraction harmonics have been calculated using the modulated structure determined by Hedoux *et al* [23] at 210 K and the ratios of the intensities calculated assuming a perfectly sinusoidal displacement pattern are listed in table 2.

The results show that the second-order diffraction harmonics can be larger than the first-order harmonics as illustrated by the $40\bar{2}+$ group of reflections in table 2. In this case the $I(-1)$ intensity corresponds to the $m = -2$ reflection of the strong primary reflection $400\bar{1}$ of column 2 of table 1. This primary reflection is very strong and so it is not surprising that the $400\bar{2}$ harmonic is larger than the weaker $40\bar{2}1$ primary reflection. Indeed the calculations suggest that whenever a primary reflection $m = \pm 1$ is strong, the higher harmonics of these reflections are also strong.

In view of this the groups of satellites having the largest primary structure factors are those which might give evidence for a discommensuration lattice especially if the primary satellites of the neighbouring Bragg reflections are weak. This is the case for the strong (400) and (600) groups of reflections. In both cases the ratios $I(-1)/I(0)$ are between 0.012 and 0.014, $I(1)/I(0)$ is less than 0.0048 and $I(-2)/I(0)$ varies between 0.0151 and 0.0085. These ratios are all much smaller than those calculated for the abrupt-discommensuration model described in section 2: 0.25 for $I(-1)/I(0)$, 0.0625 for $I(1)/I(0)$ and 0.04 for $I(-2)/I(0)$.

We conclude from this analysis that:

(a) the diffraction harmonics may play an important role, particularly for those reflections that generally have a low intensity;
(b) the abrupt-discommensuration model in which the width of the discommensurations, λ, is much less than their spacing, b, does not describe the data and a description with a common phase $\Phi(z)$ is only possible if the higher harmonics are much smaller than those given by that model.

Table 3 shows the measurements obtained for the intensities in the other plane $(0kl)$. In this plane the first-order primary satellites with $m = 1$ are absent and so on the basis of the simplest

discommensuration model, the satellite scattering should be absent. The results show that there is significant scattering. Table 3 also compares the observed scattering with that calculated using the $m = 1$ distortions found by Hedoux *et al* [23] where the calculated intensities have been scaled to give a reasonable description of the observed intensities along each line in reciprocal space. The intensities of the most intense $2q$ satellites are then reasonably reproduced by the calculations for the line with $k = 10$, but for the other values of k the calculated intensities are significantly weaker than those observed, as are the $4q$ satellites. This is evidence that higher-order distortions are needed to describe the scattering and that these cannot be described by the discommensuration model.

4. Discussion of the results

4.1. The x-ray scattering from Rb_2ZnCl_4

The x-ray scattering from Rb_2ZnCl_4 has previously been studied by Andrews and Mashiyama [11] and by Aramburu *et al* [26]. The former measured the satellites near the 600+ reflections while the latter measured the satellites between 600 and 604 and near 400+. All of the experimental results are similar to ours, except that their measurements were performed over a wider range of temperatures but only in more restricted areas of reciprocal space. Both groups of authors deduced exponents for the temperature dependence of the satellites $(T_I - T)^{2\beta}$, but except for the most intense satellite the data are too far from T_I to give reliable exponents [5].

Aramburu *et al* [26] model the data near the lock-in transition, T_L, in terms of a discommensuration model similar to that which we have used with an additional term to describe the third-harmonic $3q$ satellites which we also observed but have not discussed in detail. Aramburu *et al* [26] also used the structure determination of the modulated structure by Hedoux *et al* [23] to give the primary distortions and then modulated that distortion by an amplitude A_0 and a discommensuration density n_s which is the ratio of the volume of crystal in the discommensurations to the total volume. It is given in our notation in terms of the discommensuration width λ and spacing b as $n_s = \pi\lambda/b$. The discommensuration model then predicts that close to the lock-in transition, $b \to \infty$ while λ is independent of temperature and so $n_s \to 0$, while the abrupt-discommensuration model is valid close to the lock-in transition.

Aramburu *et al* [26] fit this model to their observed intensities and find that n_s decreases only slowly on approaching T_L and even close to T_L, n_s is about 0.25 as shown in figure 4. This is because their measurements gave higher harmonics with intensities smaller than predicted by the abrupt-discommensuration model as found in our measurements as well (section 3).

We conclude that all of the x-ray measurements on Rb_2ZnCl_4 show that the abrupt-discommensuration model does not provide an adequate description of the experimental results close to the lock-in transition. The higher harmonics of the scattering are much weaker than predicted by the theory.

4.2. Resonance measurements

Magnetic resonance techniques are a probe of the local environment of magnetic ions and have been used to study the properties of many incommensurate materials. If the modulated structure is described by a plane wave the most probable resonance frequencies are those associated with the extrema of the displacements. In contrast, the most probable resonance frequencies for a discommensuration structure are the commensurate lines. It is therefore possible to distinguish between the two models from resonance measurements [14, 41]. Unfortunately this is more complex in practice because the resonance frequency may depend on both linear and quadratic

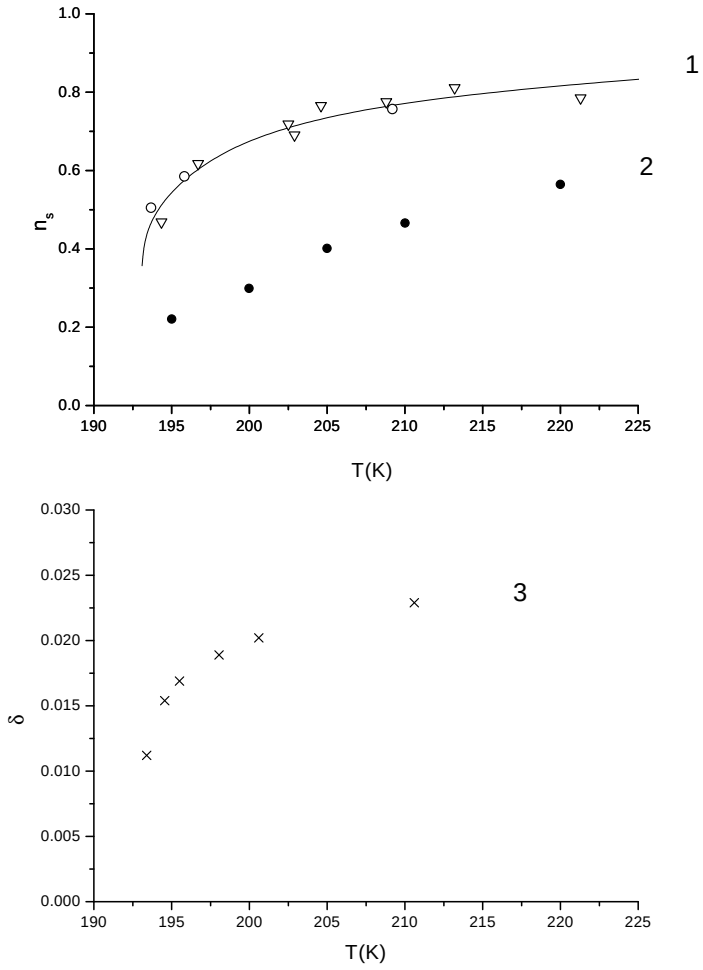

Figure 4. The temperature dependence of the discommensuration density n_s as determined by magnetic resonance techniques by Blinc *et al* [42] (1) and by x-ray scattering by Aramburu *et al* [26] (2) and of the misfit parameter δ as determined for sample 1 (3).

terms in the displacements of the atoms, and because there are a large number of unknown parameters. Initially the interpretation [41] of the data for Rb_2ZnCl_4 suggested that $n_s \rightarrow 0$ as $T \rightarrow T_L$, but a fuller more detailed study [42] of the full line-shape suggested that $n_s \approx 0.4$ at T_L; the temperature variation is shown in figure 4. Also shown in figure 4 are our measurements of the misfit parameter $\delta = 1/pb$ as a function of temperature. The figure shows firstly that the values of n_s deduced by Aramburu *et al* [26] from their x-ray measurements are considerably different from those obtained from resonance measurements [42]. This is indicative of the difficulty of determining n_s when the abrupt-discommensuration model is not adequate. The second aspect of figure 4 is illustrated by figure 5 which gives the temperature dependence of the discommensuration width as deduced from n_s/δ using the resonance data for n_s and our measurements for δ. Figure 5 shows that, within the error, λ is independent of temperature and has the value of either $(0.57 \pm 0.1)c$ or $(0.27 \pm 0.05)c$ depending on which set of measurements of n_s (figure 4) is used to determine λ.

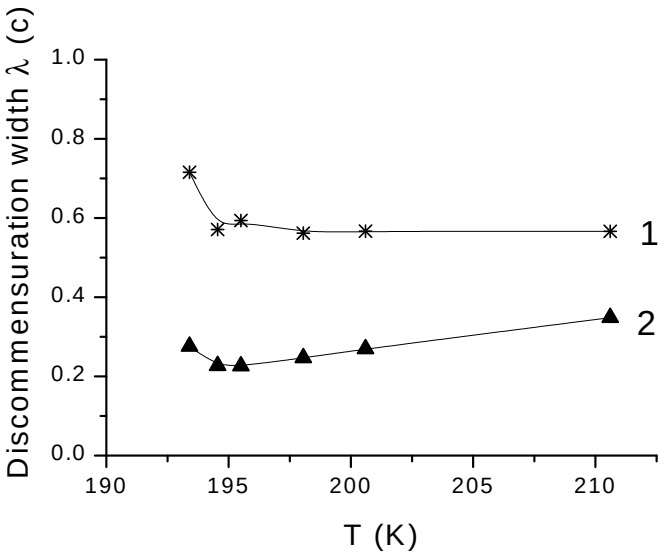

Figure 5. The temperature dependence of the domain wall width deduced from two data sets: data sets (1) and (3) of figure 4 (∗) and data sets (2) and (3) of figure 4 (▲).

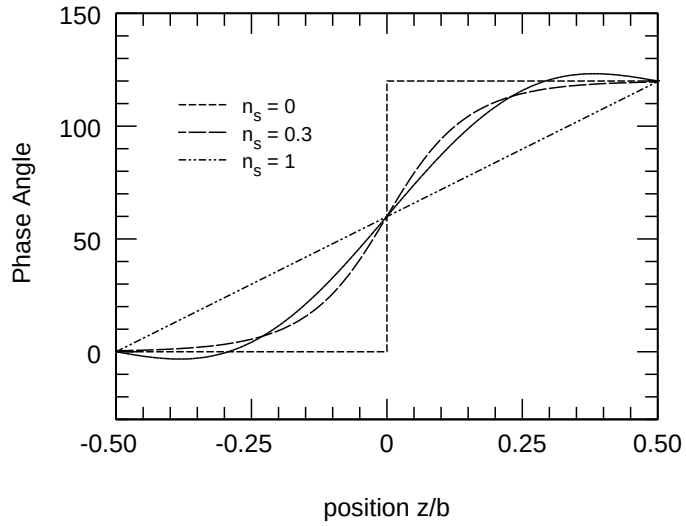

Figure 6. The spatial variation of the phase angle for different discommensuration densities n_s. The solid curve is a single-Fourier-component fit to the line with $n_s = 0.3$.

These results suggest that the higher harmonics are much smaller than are predicted by the abrupt-discommensuration model. The spatial variation of the phase angle when $n_s = 0.3$ is shown schematically in figure 6 where it is compared with the plane-wave limit $n_s = 1$ and the abrupt-discommensuration limit $n_s = 0$. The variation of the phase for $n_s = 0.3$ is very reasonably described by a single Fourier component as shown in figure 5 corresponding to only $I = 0$ and $I = -1$ components for the scattering.

4.3. Debye–Waller factors

The Debye–Waller factor for incommensurably modulated phases was first discussed by Overhauser [43] who suggested that the mth-order satellites would have a Debye–Waller factor of the form $\exp(-m^2\langle\phi\rangle^2)$ where $\langle\phi\rangle^2$ is the mean square fluctuation of the phase of the wave. This result is surprising, because unlike the conventional Debye–Waller factor it does not depend on the wave-vector transfer $\boldsymbol{Q}$ and the result strongly reduces the intensity from the higher-order satellites. Axe [44] considered the problem in more detail and showed that the phase fluctuations give displacements which vary with the atomic position such that it acts as a coupling between the scattering for different m-values, and proposed that the Debye–Waller factor might be better approximated by $\exp(-m(m-1)\langle\phi^2\rangle)$. Both of these analyses have used the nearly plane-wave formalism appropriate to temperatures close to T_I, and we are unaware of any detailed studies of the Debye–Waller factor close to T_L.

The Debye–Waller factor arising from the phase fluctuations will certainly vary with position throughout the discommensuration lattice. Nevertheless, it can be discussed assuming that the fluctuations increase the width of the discommensurations due to their fluctuations in position. The fluctuation effects on the properties of the discommensuration lattice were discussed by Bruce *et al* [8] and by Fisher and Fisher [45] for short-range interactions. For a single discommensuration the thermal fluctuations increase the fluctuation in the position of the discommensuration at temperatures above the roughening transition, logarithmically with the area of the discommensuration. When there is a lattice of discommensurations they interact and there is a corresponding fluctuation interaction which decreases exponentially with the distance between the discommensurations, while the width of the discommensurations remains finite [46]. As a result the fluctuations are not expected to alter the critical properties of the phase transition. The discommensuration lattice also interacts with the elastic strains and this [8, 47] causes a long-range attractive interaction, so the lock-in transition is of first order.

5. Summary

Measurements have been made of the x-ray scattering from Rb_2ZnCl_4 close to the lock-in transition of the incommensurably modulated phase and the commensurate ferroelectric phase. The intensities of the superlattice peaks of the satellites have been measured in several Brillouin zones and the experimental results are similar to those obtained by others [11, 26, 30].

The results have been analysed so as to determine whether a model of regularly spaced discommensurations is consistent with the measurements. This model predicts that the ratios of the satellite intensities should be the same in each Brillouin zone. The experimental results show that this is not the case. At least part of the reason for the differences is the occurrence of diffraction harmonics of the primary sinusoidal component of the structure. These were calculated from the structure determination [23] of the modulated structure and shown to account for some of the largest differences in the intensity ratios. Nevertheless, the experimental results show that the higher-order satellites are much less intense than is predicted for the abrupt-discommensuration model with $b \gg \lambda$.

The data for the $I = -1$ or $m = 2$ satellite can be described at least approximately by the discommensuration model but n_s is then about 0.3 at T_L. The intensities of the other satellites with $I = -2$, 1 or 2 differ from one Brillouin zone to another—table 2—in a way that suggests that the displacements of the atoms cannot be described by a single overall phase modulation as is inherent in the discommensuration model.

The temperature dependence of the inverse spacing between the discommensurations, $1/b$, is shown in figure 4 together with n_s which is considerably different when deduced from

x-ray [26] or magnetic resonance measurements [42]. Using the latter values of n_s and our measurements of $1/b$ suggests that the discommensuration width is temperature independent and about $0.57c$. The spacing between the discommensurations is about $5c$ at T_L.

These results show that the abrupt-discommensuration model with $b \gg \lambda$ does not provide a good description of the scattering even close to T_L. n_s is about 0.25 when a first-order transition occurs. Possibly the transition occurs due to the attractive coupling of the discommensurations through the elastic interaction while the width of the discommensurations may arise from the thermal fluctuations in their positions. It is certain that the abrupt-discommensuration model does not describe the weaker higher harmonics observed in the x-ray scattering and is a poor description of the scattering.

We suggest that this structural lock-in transition is not well described by the simple discommensuration model and that further experiments should be performed on lock-in transitions occurring at lower temperatures and with less coupling to strains.

Acknowledgments

This work was funded by the UK Engineering and Physical Sciences Research Council (EPSRC). Alexander Babkevich would like to thank the Royal Society for providing a Postdoctoral Research Fellowship. The authors thank Dr J Y Gesland (Université du Maine) and Dr K Hamano (Tokyo Institute of Technology) for sample preparation. We are grateful for helpful discussions with Dr I Aramburu (Universidad del Pais Vasco, Bilbao), Professor Dr F Frey (LMU, München), Professor D Grebille (Ecole Centrale de Paris, Châtenay-Malabry) and Professor A Yamamoto (NIRIM, Ibaraki).

References

[1] Axe J D, Iizumi M and Shirane G 1986 *Incommensurate Phases in Dielectrics* vol 2, ed R Blinc and A P Levanyuk (Amsterdam: North- Holland) p 1
[2] Cummins H Z 1990 *Phys. Rep.* **185** 211
[3] Itoh K, Hinasada A, Matsunaga H and Nakamura E 1983 *J. Phys. Soc. Japan* **52** 664
[4] Mashiyama H 1981 *J. Phys. Soc. Japan* **50** 2655
[5] Zinkin M, McMorrow D F, Hill J P, Cowley R A, Lussier J G, Gibaud A, Grübel G and Sutter C 1996 *Phys. Rev.* B **54** 3115
[6] McMillan W L 1976 *Phys. Rev.* B **14** 1496
[7] Bak P and Emery V J 1976 *Phys. Rev. Lett.* **36** 978
[8] Bruce A D, Cowley R A and Murray A F 1978 *J. Phys. C: Solid State Phys.* **11** 3591
[9] Jain S C, Harker A H and Cowley R A 1997 *Phil. Mag.* **75** 1461
[10] Cowley R A 1980 *Adv. Phys.* **29** 1
[11] Andrews S R and Mashiyama H 1983 *J. Phys. C: Solid State Phys.* **16** 4985
[12] Bestgen H 1986 *Solid State Commun.* **58** 197
[13] Tsuda K, Yamamoto N and Yagi K 1988 *J. Phys. Soc. Japan* **57** 2057
[14] Blinc R 1981 *Phys. Rep.* **79** 331
[15] Blinc R, Prelovšek P, Levstik A and Filipič C 1984 *Phys. Rev.* B **29** 1508
[16] Schneider E 1982 *Solid State Commun.* **44** 885
[17] Gesi K and Iizumi M 1979 *J. Phys. Soc. Japan* **46** 697
[18] Quilichini M and Pannetier J 1983 *Acta Crystallogr.* B **39** 657
[19] Mashiyama H, Tanisaki S and Hamano K 1981 *J. Phys. Soc. Japan* **50** 2139
[20] Mashiyama H, Tanisaki S and Hamano K 1982 *J. Phys. Soc. Japan* **51** 2538
[21] Ehses K H 1984 *Ferroelectrics* **53** 241
[22] Itoh K, Hinasada A, Daiki M, Ando A and Nakamura E 1986 *Ferroelectrics* **66** 287
[23] Hedoux A, Grebille D, Jaud J and Godefroy G 1989 *Acta Crystallogr.* B **45** 370
[24] Itoh K, Hinasada A, Daiki M and Nakamura E 1989 *J. Phys. Soc. Japan* **58** 2070
[25] Kassiba A, Bonhomme D, Fayet J C and Gibaud A 1992 *Ferroelectrics* **125** 367

[26] Aramburu I, Madariaga G, Grebille D, Perez-Mato J M and Brecşewski T 1997 *J. Physique* **7** 371
[27] Perez-Mato J M, Madariaga G, Zuñiga F J and Garcia Arribas A 1987 *Acta Crystallogr.* A **43** 216
[28] Gaillard V B, Chapuis G, Dusek M and Petříček V 1998 *Acta Crystallogr.* A **54** 31
[29] Cowley R A and Bates S 1988 *J. Phys. C: Solid State Phys.* **21** 4113
[30] Aramburu I, Madariaga G and Perez-Mato J M 1995 *J. Phys.: Condens. Matter* **7** 6187
[31] Shiba H and Ishibashi Y 1978 *J. Phys. Soc. Japan* **45** 409
[32] Scott A C, Chu F Y F and McLaughlin D W 1973 *Proc. IEEE* **61** 1443
[33] de Wolff P M 1974 *Acta Crystallogr.* A **30** 777
[34] Janner A and Janssen T 1977 *Phys. Rev.* B **15** 643
[35] Wolff P M, Janssen T and Janner A 1981 *Acta Crystallogr.* A **37** 625
[36] Yamamoto A and Nakazawa H 1982 *Acta Crystallogr.* A **38** 79
[37] Yamamoto A 1982 *Acta Crystallogr.* A **38** 87
[38] Yamamoto A 1996 *Acta Crystallogr.* A **52** 509
[39] Prelovšek P and Blinc R 1984 *J. Phys. C: Solid State Phys.* **17** 577
[40] Hedoux A, Grebille D, Lefebvre J and Perret R 1989 *Phase Transitions* **14** 177
[41] Blinc R, Rutar V, Topič B, Milia F, Aleksandrova I P, Chaves A S and Gazzinelli R 1981 *Phys. Rev. Lett.* **46** 1406
[42] Blinc R, Rutar V, Topič B, Zumer S, Seliger J, Aleksandrova I P and Milia F 1986 *J. Phys. C: Solid State Phys.* **19** 3421
[43] Overhauser A W 1971 *Phys. Rev.* B **3** 3173
[44] Axe J D 1980 *Phys. Rev.* B **21** 4181
[45] Fisher M E and Fisher D S 1982 *Phys. Rev.* B **25** 3192
[46] Bruce A D and Cowley R A 1978 *J. Phys. C: Solid State Phys.* **11** 3609
[47] Lajzerowicz J and Levanyuk A P 1994 *Phys. Rev.* B **49** 15 475